CHALMERS

Structural Analysis of Support Structures for Industrial Cooking Pans

A Finite Element Study of the GS23 Series

Bachelor's thesis in Industrial and Materials Science

Emil Vatsöy

Department of Industrial and Materials Science

CHALMERS UNIVERSITY OF TECHNOLOGY
Gothenburg 2026
www.chalmers.se

Bachelor's Thesis 2026

Structural Analysis of Support Structures for Industrial Cooking Pans

A Finite Element Study of the GS23 Series

Emil Vatsöy

CHALMERS

Department of Industrial and Materials Science
Chalmers University of Technology
Gothenburg 2026

Structural Analysis of Support Structures for Industrial Cooking Pans
A Finite Element Study of the GS23 Series
Emil Vatsöy

Supervisors: Björn Andersson and Magnus Ekh, Chalmers University of Technology
Examiner: Magnus Ekh, Computational Mechanics and Materials Engineering

Bachelor's Thesis 2026
Department of Industrial and Materials Science
Chalmers University of Technology
SE-412 96 Gothenburg
Telephone +46 31 772 1000

Cover image: Industrial cooking pans from Steeltech arranged in a series configuration.

Written in LaTeX
Gothenburg 2026

Structural Analysis of Support Structures for Industrial Cooking Pans
A Finite Element Study of the GS23 Series
Emil Vatsöy
Department of Industrial and Materials Science
Chalmers University of Technology

Abstract

This study presents structural analyses of the right-side support structures used in the GS23 series of industrial cooking pans developed by Steeltech. The analyses were performed using the finite element method (FEM) to assess stress, deformations, and structural stability under representative static load cases. Two support structure variants were considered, corresponding to pan sizes of 150-300 L and 50-100 L, respectively.

The results show that both structures are conservatively dimensioned, with all stress levels remaining below the material yield strength of 252 MPa. The safety factors were approximately 3.2 for the 150-300 L structure and 3.6 for the 50-100 L structure. The most critical region in both designs was identified at the motor mounting hole. The stress levels always remained within acceptable limits.

A linear eigenvalue buckling analysis showed high load multiplier factors, suggesting that both structures are far from their critical buckling loads. The maximum total deformation was small in all load cases and is not expected to affect performance.

A thickness sensitivity study showed that the 150-300 L structure is sensitive to thickness reductions of rectangular hollow sections (RHS) beams below 2 mm, where stresses increase significantly. The 50-100 L structure is less sensitive and shows no significant increase in stress when the RHS beam thickness is reduced from 3 mm to 1.5 mm. This suggests potential for material savings.

The current designs provide sufficient structural performance under the considered load cases. While optimisation potential exists through thickness reduction, greater improvements may be achieved through design modifications aimed at manufacturing efficiency.

Keywords: Finite element analysis, structural analysis, cooking pans, stress analysis, buckling, deformation, thickness optimisation.

Acknowledgments

I would like to thank my supervisors at Chalmers University of Technology, Björn Andersson and Magnus Ekh, for their guidance and valuable feedback throughout the project.

Emil Vatsöy, Göteborg, May 2026

Acronyms

Below is the list of acronyms that have been used throughout this thesis listed in alphabetical order:

FEA	Finite element analysis
FEM	Finite element method
LMF	Load multiplier factor
RHS	Rectangular hollow section

Contents

List of Figures

List of Tables

1
Introduction

1.1 Background

Commercial kitchens and the food industry place high demands on their production equipment. The equipment must be robust, reliable, and meet strict hygiene requirements (Swedish Institute for Standards, 2005). Commercial kitchens rely on cooking pans to efficiently prepare large amounts of food (U.S. Environmental Protection Agency, 2023). During their operational lifetime, these pans are exposed to both mechanical and thermal stresses, such as static loads from filled vessels, dynamic loads during operation, and repeated thermal cycles during heating and cooling (Saravacos & Kostaropoulos, 2016).

Steeltech is a company specialised in the development and manufacturing of cooking pans for industrial applications (Steeltech i Alingsås AB, 2026b). The cooking pans are mounted on a horizontal axis, which is supported by two support structures. Both support structures carry half the vertical load during operation. One of them also integrates functional components such as the control electronics, user interface, and a drive system that enables the rotation of the pan. This rotation function allows the pan to empty its contents and facilitates cleaning after the cooking process (Steeltech i Alingsås AB, 2026a).

Steeltech is developing the GS23 series, a new generation of stainless steel cooking pans with volumes of 50, 80, 100, 150, 200, and 300 litres. The series is intended to complement and later replace existing models, meeting both functional, economic, and customer requirements (Rexander, 2026). As a series-produced product, design decisions made at this stage have long-term implications for manufacturing efficiency, cost, and product performance (O'Driscoll, 2002).

A central part of the design of the cooking pan is the support structure that integrates the control and drive systems, as seen in Figure 1.1. This structure carries a significant portion of the operational loads and ensures sufficient strength, stiffness, and stability over the product's service life.

The current design of the GS23 series load-bearing structures is largely based on previous versions and accumulated experience rather than verified strength and stiffness calculations or finite element simulations. This is common in industrial product development, where the use of detailed analysis methods is often limited by time

and cost constraints (Davis et al., 2013). While this approach reduces development time, it may result in over- and under-dimensioning. Over-dimensioning increases material usage and cost, while under-dimensioning can compromise structural safety and performance (Eckert & Ola, 2017), both are undesirable from both ethical and environmental perspectives. Despite this, no systematic structural evaluation of the GS23 support structure has yet been performed.

These factors highlight the need for a systematic structural assessment of the GS23 support structure using numerical methods. Such an analysis enables the evaluation of structural performance and supports decisions related to material usage and potential design improvements.

Currently, the different support structure sizes are based on two designs, as seen in Figure 1.1:
a) A larger support structure shared by the 150, 200, and 300 litre pans.
b) A smaller support structure shared by the 50, 80, and 100 litre pans.

a) GS23 support structure shared between models 150, 200 and 300 litres.

b) GS23 support structure shared between models 50, 80 and 100 litres.

Figure 1.1: Side-by-side comparison of the larger (a) and smaller (b) support structures used in Steeltechs cooking pans.

1.2 Purpose

The primary purpose of this work is to evaluate the structural integrity of the support structure in the GS23 series of industrial cooking pans. The evaluation is performed using finite element analysis (FEA) to determine stresses and deforma-

tions, as well as structural stability under representative load cases.

The study aims to assess whether the current design is adequately dimensioned with respect to structural safety and material usage. The study seeks to identify potential over- or under-dimensioning, as well as opportunities for reducing material usage and cost while maintaining structural integrity.

1.3 Research Questions

- Is the current load-bearing structure over- or under-dimensioned for the typical operational load case?
- Which areas are critical with respect to stress levels, deformation, and buckling?
- Can material thickness be reduced without compromising safety?
- How do the results inform potential improvements in the structural design?

1.4 Limitations

- The effects of residual stresses due to welding are not considered.
- Welded joints are not modelled in detail.
- Stresses in the lid, pan, cladding, and smaller side support structure are not analysed.
- Thermally induced stresses are not included.
- Vibration and dynamic effects are not considered.
- Modal analysis is not performed.
- Not all possible load cases are evaluated; only selected worst-case scenarios are considered.
- Detailed sensitivity analysis of boundary condition assumptions is not performed.

2

System Configuration and Methodology

This chapter describes the system and methodology used to analyse the support structures response under operational loads. The chapter outlines a description of the cooking pan and its support structure, as well as the modelling assumptions, material properties, boundary conditions, modelling strategies, and the finite element method used to evaluate stresses, deformations, and structural stability in the support structure.

2.1 System Overview

The system considered in this study is shown in Figure 2.1. The cooking pan rests on the side structures and transfers its weight through them. The focus of this study is the right-hand support structure, which will be analysed in detail.

Figure 2.2 shows the right-hand support structure without its sheet metal cladding, cover plates, and electronics. This CAD model is the geometry used in the finite element analysis (FEA), with all non-structural components removed from the CAD model. The aim of the analysis is to evaluate the structural response under operational loads and identify possible regions of high stress or large deformation.

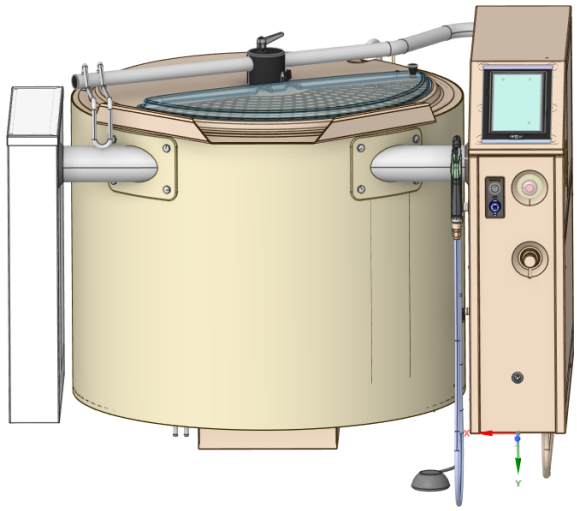

Figure 2.1: The 300 L cooking pan mounted on both support structures.

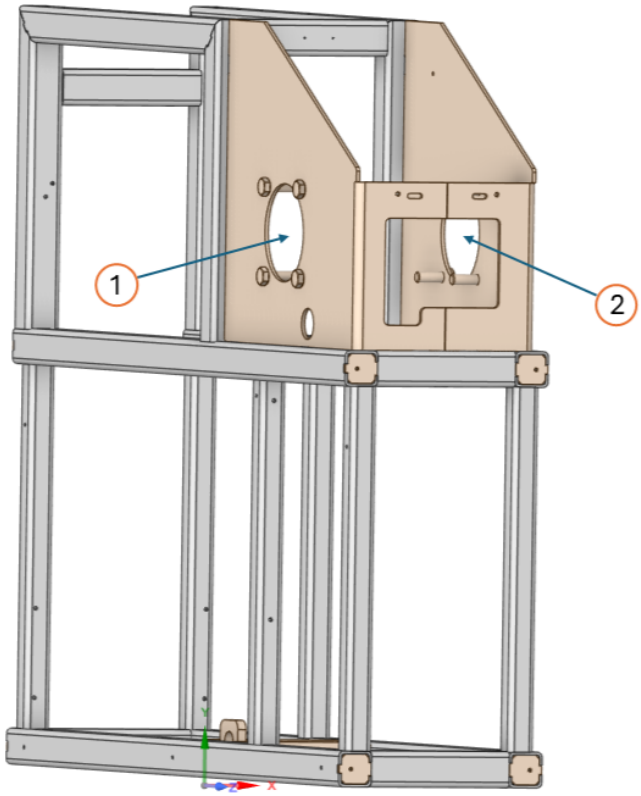

Figure 2.2: Load-bearing structure with support axis holes visible indicated by highlights 1 and 2.

2.2 Structural Configuration and Load Transfer

The pan is mounted on an axis which is supported by a framework on both sides of the pan. This supporting framework consists of rectangular hollow section (RHS) beams and sheet metal, both in stainless steel. Moreover, in one of these supporting frameworks, the tilting of the pans is controlled by a hydraulic cylinder that rotates the axle (see Figure 2.4). This allows the pan to rotate about the support axis from an upright position to a fully tilted position, corresponding to tilt angles $\theta = 0°$ (upright) to $\theta = 92°$ (fully tilted).

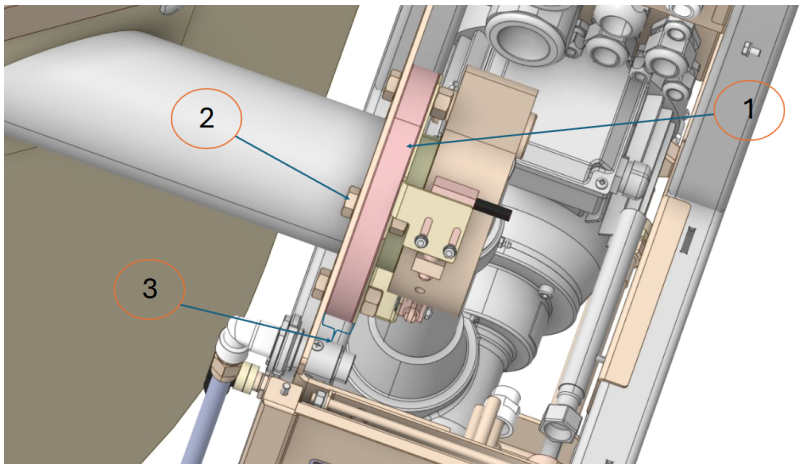

Figure 2.3: Overview of the bearing assembly. Highlights indicate: (1) the bearing, (2) the bolt securing the bearing to the plate, and (3) the bearing length.

The axle is mounted through a circular opening in the sheet metal side plate of the structure (see highlight 1 in Figure 2.2), where a bearing transfers the load from the pan to the support structure (see Figure 2.3). Due to symmetry, the vertical loads from the cooking pan are shared between the two support structures.

The cooking pans can be mounted individually or in series with an adjacent pan. In single pan configurations, only the primary load-bearing hole (see Figure 2.2, highlight 1) is loaded. When two pans are connected in series, the secondary hole (see Figure 2.2, highlight 2) is also loaded, resulting in additional load cases.

In the series configuration, the adjacent pan transfers only vertical loads through the secondary mounting hole, while no moment is transferred, as the connection allows free rotation around the axis.

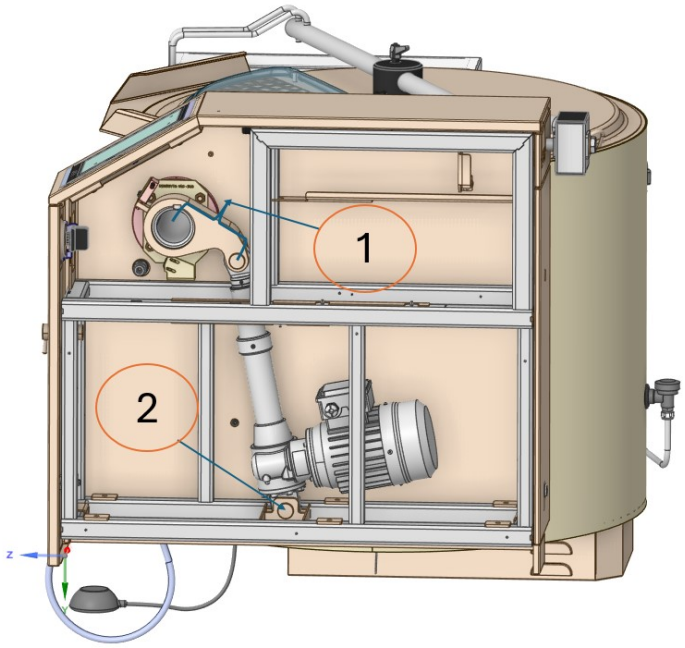

Figure 2.4: This figure shows how the cooking pan balances the moment generated by pans gravity. Highlights show: (1) tilting motor's lever arm, (2) Tilting motor connection to support structure.

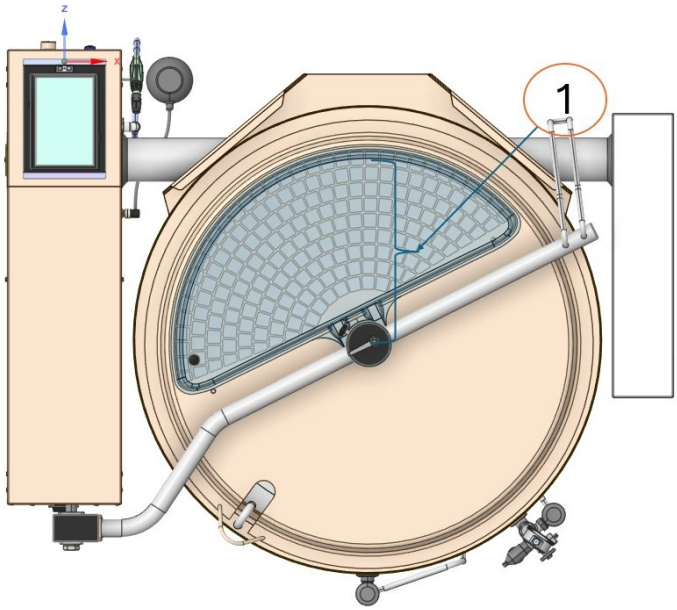

Figure 2.5: Top view of the 300 L pan. Highlight 1 marks the eccentric position of the supporting axis relative to the pans centre of gravity.

At the lower central region of the structure, a tilting motor is mounted (see Figure 2.4, highlight 2). Due to the eccentric position of the axle relative to the pan's centre of gravity (see Figure 2.5, highlight 1), the gravitational force generates a moment around the support axis. This moment is entirely resisted by the analysed support

structure through a lever arm (see Figure 2.4, highlights 1 and 2), as the opposite side is only connected via a bearing and cannot resist moments.

2.3 Finite Element Analysis

The Finite Element Method (FEM) is a numerical method for approximating solutions to differential equations. The idea is to divide a complex problem into smaller pieces known as elements, which are connected through nodes. Within each element, the unknown field variables are approximated using interpolation functions defined by the nodal values (Zienkiewicz and Taylor, 2005). The element equations are then assembled into a matrix system representing the entire structure. By solving this system, unknowns such as temperature, displacements, and stresses can be determined throughout the model (Jagota et al., 2013).

In this study, FEM is applied to evaluate stresses, deformation, and structural stability of the support structure under static loads. The discretisation of the structure into elements forms the mesh used in the analysis.

2.3.1 Modelling Assumptions

This study uses an elastic-plastic material model with bilinear isotropic hardening, i.e., a linear elastic material response below the initial yield limit and plastic deformation with a constant tangent modulus when loaded above the yield limit. Relevant to this study, the modelling allows for local load redistribution in the case of plastic deformations in highly stressed local regions. The material is assumed to be isotropic, meaning that any anisotropic effects from manufacturing, of either RHS or sheet metal, are not accounted for.

To evaluate the structural response of the support structure under static loads, the model will be analysed using the Finite Element Method (FEM). The geometric simplifications and modelling choices required for the FEM analysis are described in detail in Section 2.3.2. All components are made of stainless steel EN 1.4301, and the material properties used in the analysis are listed in Table 2.1, based on Ansys Granta EduPack data for EN 1.4301 (Ansys, Inc., 2026).

Table 2.1: Material properties for stainless steel EN 1.4301 used for structural analysis.

Property	**Symbol**	**Value**
Young's Modulus	E	196 GPa
Poisson's Ratio	ν	0.269
Yield Strength	σ_y	252 MPa
Density	ρ	$7954\,\mathrm{kg/m^3}$
Plastic Tangent Modulus	E_t	1220 MPa
Temperature of analysis	T	23 °C

Both RHS and sheet metal are modelled using their mid-surfaces since the thickness is small relative to the other dimensions. This follows a conventional engineering approach, where small geometric features, such as small holes, radii, and weld fillets are not included. This enables the use of shell elements, reducing computational cost while preserving the overall structural response, but it limits the representation of three-dimensional stress effects, specifically the through-thickness stress variation. Weld-induced residual stresses are also neglected, as the focus of this study is on global structural behaviour rather than local weld performance.

Friction between contacting surfaces is neglected because its influence on the global load transfer is considered negligible. This is done to simplify the model while maintaining an accurate representation of the structural behaviour. Temperature effects are also neglected, and the analysis is performed under the assumption of a constant temperature of 23 °C. This is justified as the study focuses on mechanically induced loads, and no significant temperature changes occur in the structure during operation.

Half of the pans weight is applied to the analysed support structure, assuming symmetric load distribution between the two supports. The load is transferred from the pan through the axle and bearing (see Figure 2.3) to the mounting holes (see Figure 2.2), where it is introduced in the model as a distributed load at one or both holes, depending on the configuration. The weights of auxiliary components such as cables, electrical boxes, and the tilting motor is also not included explicitly. These contributions are small relative to the primary loads of the pan and are therefore simply accounted for by the use of load factors.

As the cooking pan tilts around its axis, it is assumed that it always remains fully filled, even though the contents may begin to spill. This is conservative to represent a worst case scenario, such as a viscous or sticky liquid that may remain in the pan during tilting.

Only static loads are considered, whereby no dynamic effects on the structure are taken into account. This assumption is supported by observations of the system, where no significant jerking or impulsive loading occurs during tilting or start/stop operations. However, neglecting dynamic effects may still lead to an underestimation of the predicted peak stresses during operating conditions.

2.3.2 Finite Element Method Implementation

To simulate the load scenarios, Ansys (Ansys, Inc., 2024c) was chosen as the FEA software to model and analyse the structural response in this study. The CAD geometry was originally created by Steeltech in Inventor (Autodesk, Inc., 2026), and then exported to Ansys. Since only the effects of static loads are being studied in this project, the analysis module "Static structural" was used.

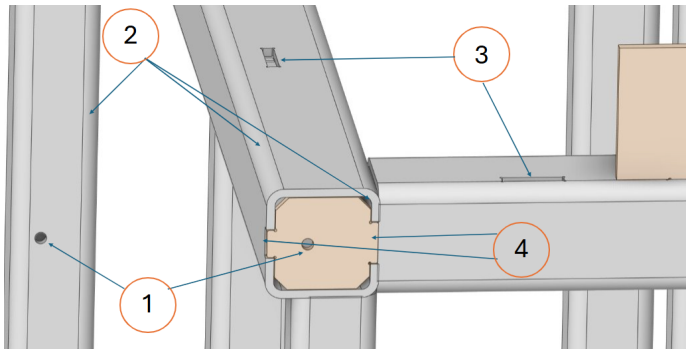

Figure 2.6: Number 1-4 shows example of locations where chamfers, holes and installation tabs were removed.

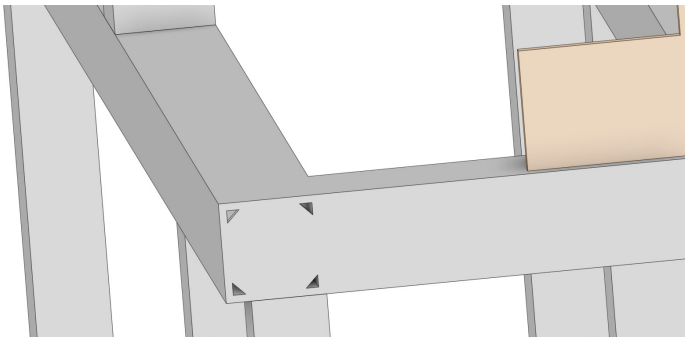

Figure 2.7: Same structure as in Figure 2.6, after unnecessary features were removed.

The models were examined in the Ansys CAD programme SpaceClaim (Ansys, Inc., 2024a) to assess which components should be kept and which geometrical features required modification. The objective was to create an FE model that is both computationally efficient and structurally accurate, minimising computational cost by omitting components of none or negligible structural significance. Examples of such components and features are small holes, installation tabs, and other non-structural components. Gaps or overlaps between beams and all chamfers were also removed. A before and after comparison is shown in Figures 2.6 - 2.7. These alterations resulted in a simpler model without compromising the load paths or structural stiffness.

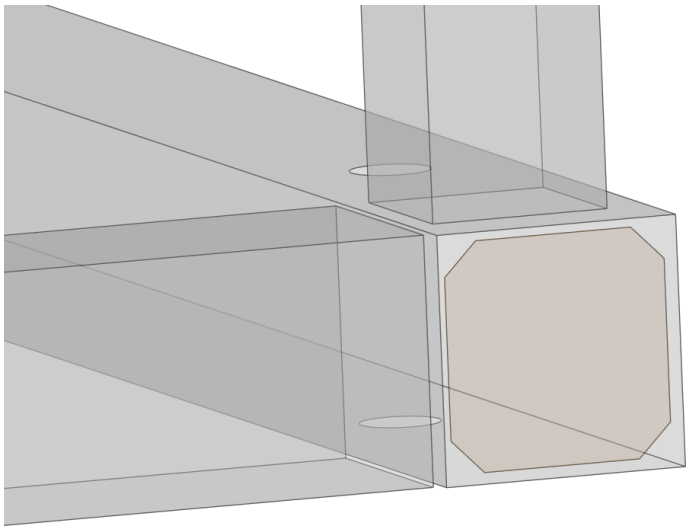

Figure 2.8: Mid-surface representation showing how gaps form between parts after conversion.

Note that when representing a thin-walled 3D structure with 2D mid-surface elements, the thickness of the structure is a property of the FE-element. Moreover, when constructing the mid-surface model, minor adjustments are necessary for the surfaces of adjacent components to align and join. This is exemplified in Figure 2.8.

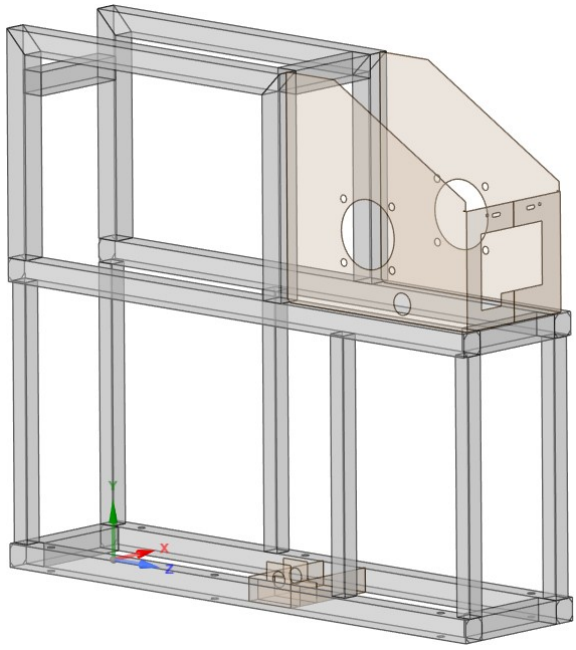

Figure 2.9: Support structure after mid-surface conversion.

Figure 2.9 shows the structure after geometric simplifications and mid-surface conversion. The connections between parts are modelled as fully bonded using the Share Topology tool (Ansys, Inc., 2024b).

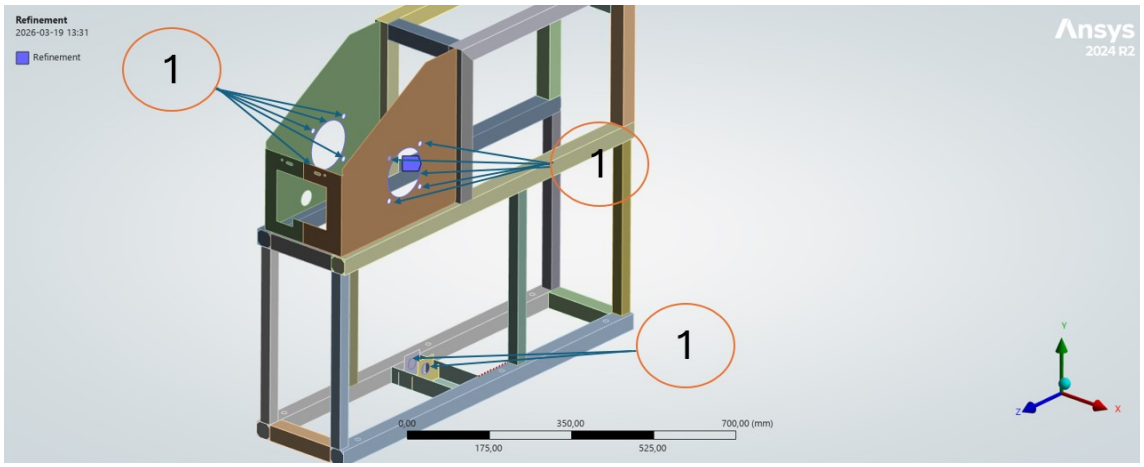

Figure 2.10: Locations of local automatic mesh refinements.

The geometry was meshed using shell elements with a typical element size of 3 mm. Local automatic mesh refinements were applied in regions of expected high stress (see highlights in Figure 2.10). A convergence study based on the equivalent (von Mises) stress was conducted to ensure mesh-independent results, with a maximum allowable change of 5%. The applied mesh strategy ensures that the stress distribution is accurately captured in critical regions while maintaining a reasonable computational cost.

Due to geometric idealisations, local stress singularities may be observed at sharp geometric discontinuities. The stresses in these regions increase with mesh refinement and do not converge, indicating non-physical behaviour. To obtain physically meaningful results, stresses will be evaluated at locations approximately half a material thickness away from these discontinuities, where the stress values stabilise and the mid-surface conversion thickness parameter is taken into account. As a result, non-physical peak stresses at geometric singularities are not used for evaluation.

2.4 Boundary conditions

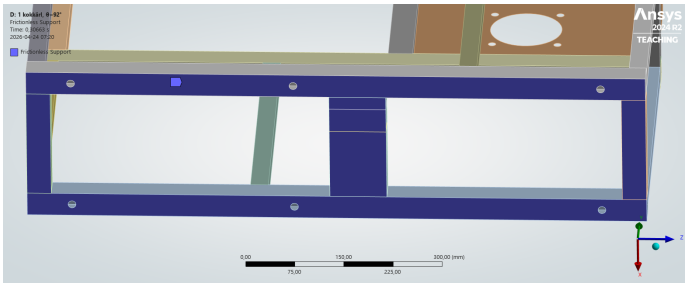

Figure 2.11: Frictionless support boundary condition applied to the underside of the support structure. The constrained surface is highlighted in blue

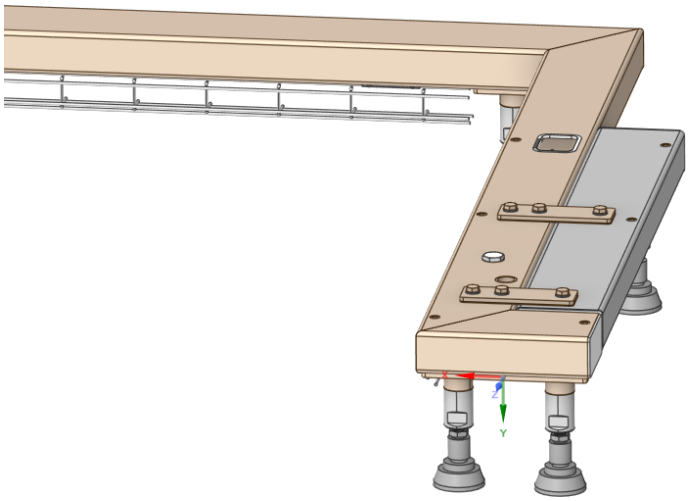

Figure 2.12: The base on which the pans support structure stands.

The support structure is constrained using frictionless supports applied to the underside of the support structure (see Figure 2.11), preventing displacement normal to the contact surface while allowing in-plane movement. This approximates the physical contact between the base (see Figure 2.12) and the support structure while neglecting friction.

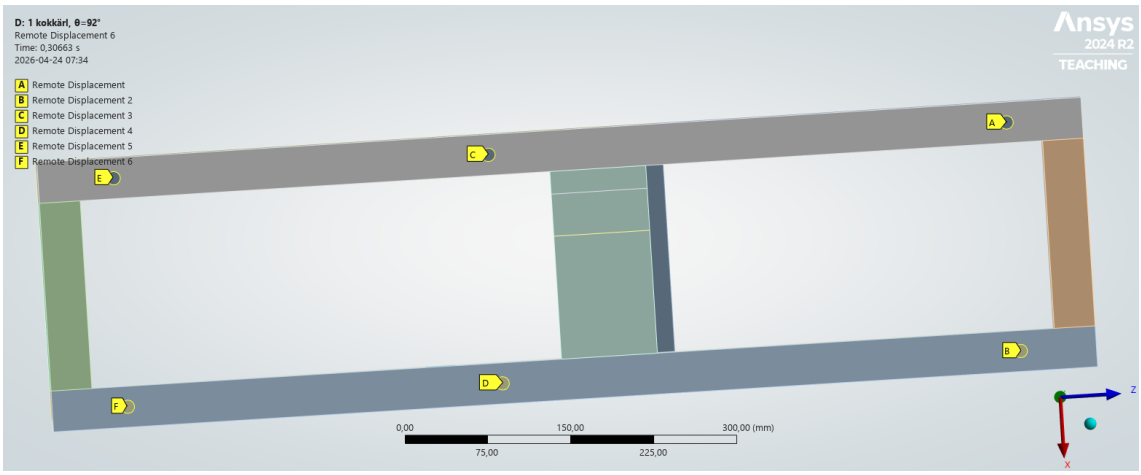

Figure 2.13: Boundary constraint along the bottom boltholes, restricting translation.

Additional constraints are applied at the bolt hole locations (see Figure 2.13), where in-plane-translations are restricted to prevent rigid body motion while allowing rotational flexibility.

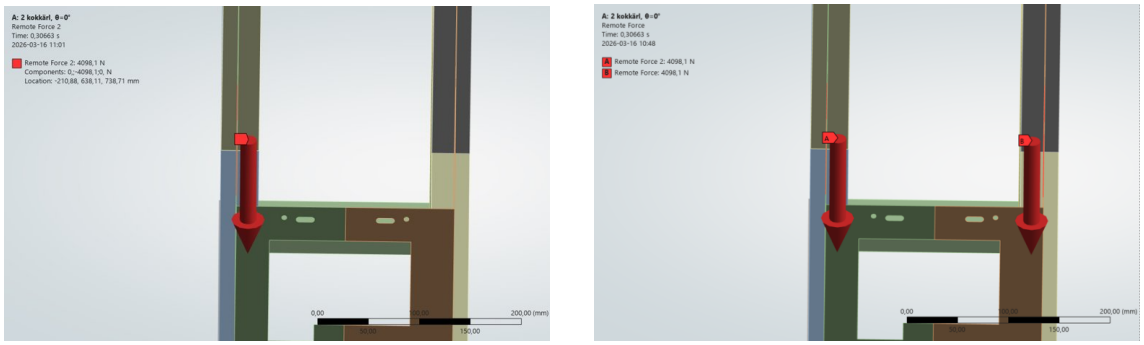

(a) **(b)**

Figure 2.14: Comparison of load application for single and series-connected cooking pans. (a) shows the single-pan configuration, and (b) the series configuration.

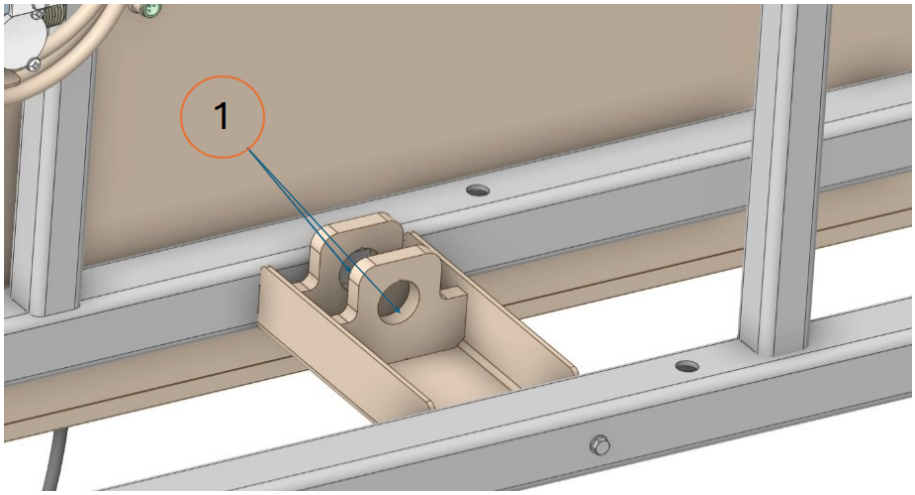

Figure 2.15: (1) Close up of where the tilting motor is attached to the structure.

The load from the cooking pan is transferred through the axle and bearing to the mounting holes in the side plate (see Figure 2.14). The load is applied at one or both mounting holes depending on the configuration. Since the load is transferred through the bearing, it acts at a distance from the plate corresponding to half the bearing width. This introduces a lever arm, resulting in both force and moment in the structure.

The moment generated by the pans weight is balanced by the tilting motor and is represented by a force applied at the motor connection points (see Figure 2.15). The load direction follows the angle of the tilting motor. In addition, gravity is applied as an acceleration acting on the structure.

The boundary conditions represent a simplified model of the real support and loading conditions.

2.5 Load Cases

The structural response is evaluated for a set of representative load cases corresponding to different operating conditions. The loads are based on the pans weight and the forces generated during tilting.

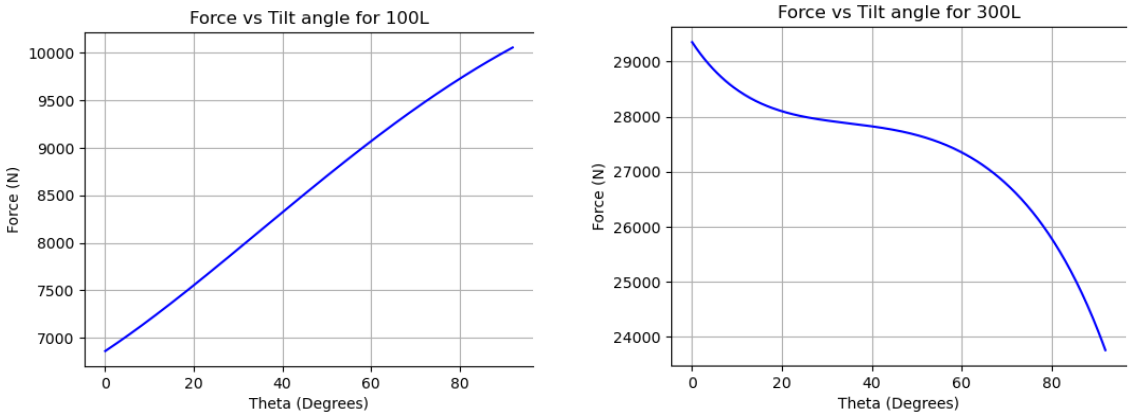

a) Force for 100 L cooking pan.

b) Force for 300 L cooking pan.

Figure 2.16: Calculated force at the tilting motor connection point as a function of pan tilt angle for 100 L and 300 L pans.

The force at the tilting motor connection varies with the tilt angle θ due to the changing position of the centre of gravity and angles changing with θ . This relationship is shown in Figure 2.16. The relationship between force and tilt angle depends on the geometry and the position of the centre of mass, which differs between the two support structure sizes.

The gravitational moment from the pan is given by

$$M_g(\theta) = mgL_r \cos(\alpha_r + \theta)$$

The corresponding motor force is then calculated as

$$F_{\text{motor}}(\theta) = \frac{M_g(\theta)}{L_{\text{small}} \sin(\gamma(\theta))}$$

where m is the pans mass, g is the gravitational acceleration, L_r is the distance from the tilt axis to the centre of mass of the pan, α_r is the initial angle of the centre of mass lever arm, L_{small} is the lever arm from the axis to the connection point, and $\sin(\gamma(\theta))$ accounts for the changing geometry of the mechanism during tilting.

To ensure a conservative analysis, the loads are scaled according to Eurocode 0 (SS-EN 1990:2023) (Svenska institutet för standarder (SIS), 2023). A load factor of 1.35 is applied to permanent loads and 1.5 to variable loads.

Only the most critical configurations are considered. For the larger (150–300 L) and smaller (50–100 L) support structures, the 300 L and 100 L pans are analysed, respectively.

The following load cases are evaluated for both sizes:

- Single pan mounted on the structure with $\theta = 0°$ (upright position).
- Single pan mounted on the structure with $\theta = 92°$ (fully tilted position).
- Two pans connected in series and mounted on the structure with $\theta = 0°$.
- Two pans connected in series and mounted on the structure with $\theta = 92°$.

These cases represent the most critical loading conditions, corresponding to the minimum and maximum moments generated by the pan due to the tilt angle θ. Detailed load magnitudes are provided in Appendix C.

2.6 Linear Eigenvalue Buckling Analysis

The structural stability of the support structures was evaluated using a linear eigenvalue buckling analysis based on the pre-stressed state obtained from the static structural solution.

The analysis determines a set of buckling modes (eigenvectors) and corresponding load multiplier factors (eigenvalues, LMFs). The LMF represents the factor by which the applied loads must be multiplied for the structure to reach the theoretical buckling load, where the lowest LMF is used to assess the critical buckling load. For each load case, the first 15 buckling modes were extracted.

For the buckling analysis, the material model was simplified to linear elastic behaviour since the linear eigenvalue buckling formulation assumes an elastic material response.

Linear eigenvalue buckling analysis is based on an idealised structural model with perfect geometry. The predicted buckling loads, therefore, correspond to theoretical values. In practice, real structures are sensitive to imperfections such as geometric deviations, and even small deviations from the ideal configuration can lead to a reduced buckling capacity. As a result, the LMF from linear eigenvalue buckling analysis may be non-conservative, i.e. higher than those observed in reality (COMSOL AB, 2014).

3
Results

This chapter presents the results from the FEA of the GS23 support structures. The results are organised by pan size group (150–300 L and 50–100 L) and by load case. For each case, the structural response is evaluated using the von Mises equivalent stress and compared to the material yield strength to evaluate safety factors. The total deformation is also evaluated to assess structural stiffness, and a linear eigenvalue buckling analysis is used to evaluate structural stability. In addition, a thickness sensitivity study is performed to evaluate the influence of RHS thickness on the structural response.

A mesh convergence study was performed to ensure a mesh independent evaluation of the results. As expected, stress singularities were observed, and the equivalent (von Mises) stress did not always converge with mesh refinement. These non-physical stresses were excluded from evaluation by analysing the stress at points previously defined in Section 2.3.2. Here, the stress values changed by less than 5% between the two mesh refinements, indicating mesh-independent results. A convergence curve demonstrating mesh independence is provided in Figure B.1 in Appendix B.

3.1 Stress Distribution for 150-300 L

The stress distribution for the 150–300 L support structure is presented for the load case with the highest load magnitude as this case is expected to produce the highest stress levels. The most critical load case corresponds to two pans connected in series with a tilt angle $\theta = 0°$. To improve visualisation, the colour scale is rescaled to 100 MPa, with all stresses above this value shown in red.

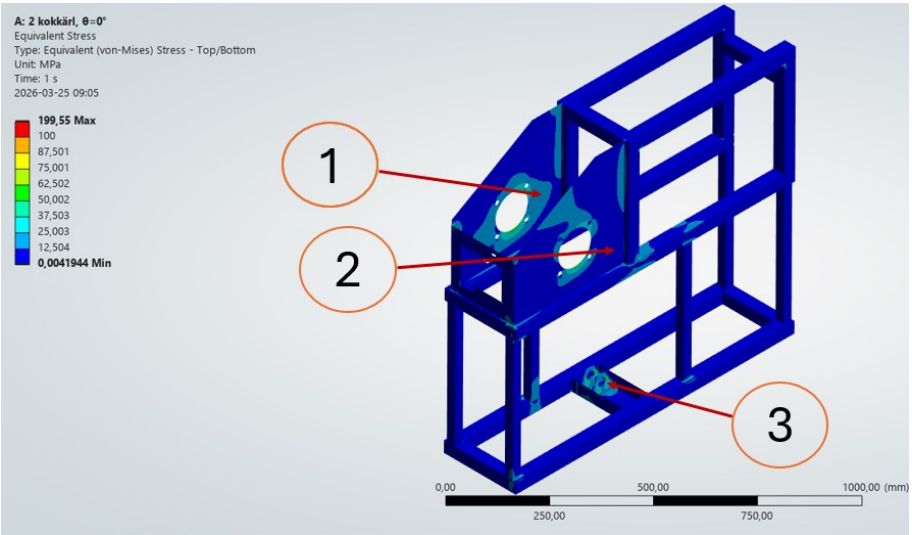

Figure 3.1: Isometric view of the 150-300 L support structure showing von Mises stress for the most critical load case. The highlighted general Regions (1-3) are examined in more detail in subsequent figures.

Figure 3.1 shows the global stress distribution for the selected load case. Elevated stress levels are observed in several regions of the structure. The remaining areas exhibit low stress levels, indicating that the load is primarily carried through Regions 1-3. These most critical regions of the structure are highlighted in Figure 3.1 and are examined in more detail in Figures 3.2 - 3.4.

Probe locations were selected based on the global stress distribution and the main load paths of the structure, with a focus on regions of elevated stress near load-carrying connections. The evaluation points were placed approximately half a material thickness (approximately 1.5 mm) away from geometric discontinuities.

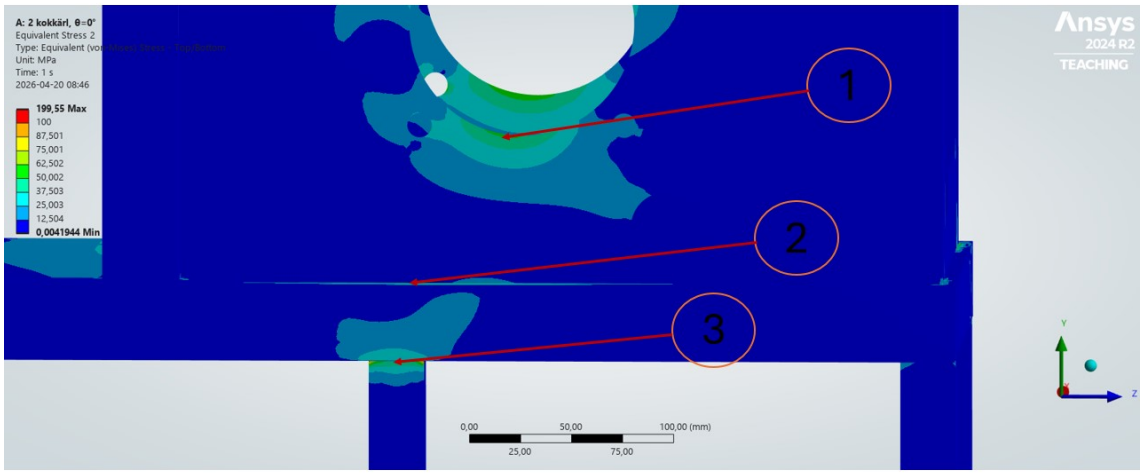

Figure 3.2: Local stress distribution in Region 1 showing equivalent von Mises stress for the case with the highest external loads. The highlighted locations (1-3) indicate selected points for evaluation: (1) Left hole bottom, (2) Left horizontal beam top, and (3) Left support beam.

Three probe locations were selected to evaluate the stress levels in Region 1 (see Figure 3.2). The evaluated stresses range from 40 to 53 MPa. The higher stresses are observed at location (1) Left Hole Bottom (52 MPa) and location (3) Left Support Beam (53 MPa).

The load is introduced at the mounting hole and transferred into the surrounding structure without causing high local stress concentrations. The relatively low stress level at location (2) Left Horizontal Beam Top (40 MPa), along with Figure 3.2 shows that the load is distributed along the horizontal beam and ultimately transferred to the left support beam.

The maximum stress in Region 1 is 53 MPa, corresponding to a safety factor of approximately 4.7 against yielding. Region 1 appears conservatively dimensioned under the considered load case.

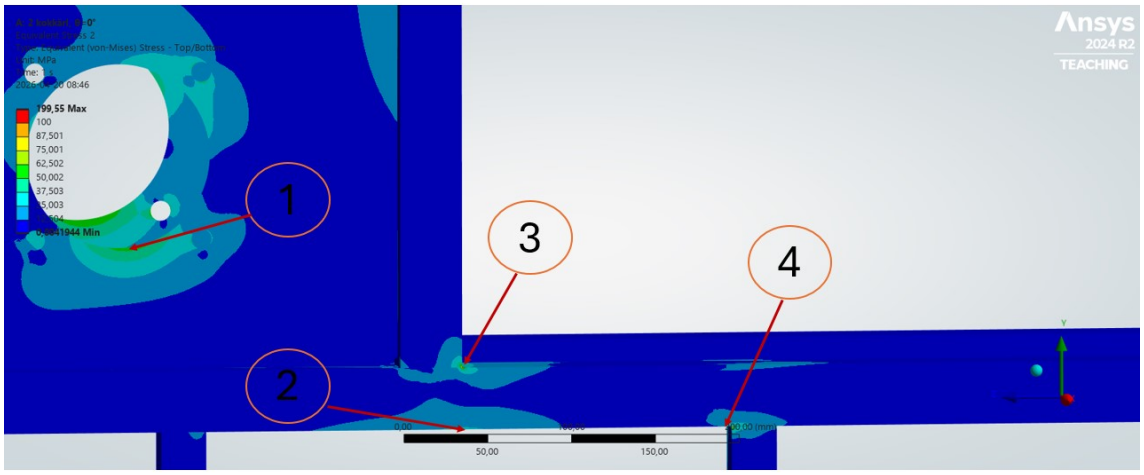

Figure 3.3: Stress distribution in Region 2 showing equivalent von Mises stress. The highlighted locations (1-4) indicate selected points for evaluation: (1) Right Hole Bottom, (2) Right Horizontal Beam Bottom, (3) Right Horizontal Beam Top, and (4) Right Support Beam.

In region 2 (see Figure 3.3), the highest stress of 54 MPa is located at (1) Right Hole Bottom. The stress distribution clearly indicates bending behaviour in the horizontal beam, with higher stresses observed at (3) Right Horizontal Beam Top (31 MPa) compared to (2) Right Horizontal Beam Bottom (22 MPa).

The load transferred through the right mounting hole introduces a bending moment due to the offset between the mounting hole and the (4) Right Support Beam. The lower stress of 23 MPa at location (4) suggests that the load is distributed through the horizontal beam and shared between multiple load paths, i.e the vertical beams below.

Despite this, the stress levels remain relatively low, with a safety factor of 4.6 against yielding. Similar to Region 1, Region 2 is conservatively dimensioned under the considered load case.

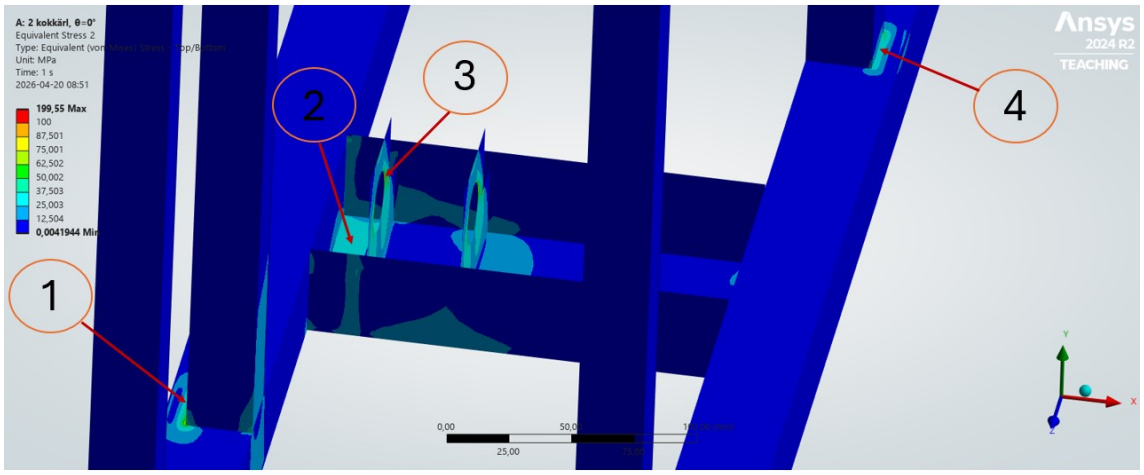

Figure 3.4: Stress distribution in Region 3 showing equivalent von Mises stress. The highlighted locations (1-4) indicate selected points for evaluation: (1) Left Support Beam Bottom, (2) Motor Mount Beam, (3) Motor Mounting Hole, and (4) Right Support Beam Bottom.

Four probes were selected to evaluate the stress levels in Region 3 (see Figure 3.4). The highest stress of 77 MPa is observed at location (3), Motor Mounting Hole, making this the most critical location in the structure. This is expected, as the motor mounting hole is responsible for balancing the moment generated by the eccentric position of the pan's centre of gravity.

Lower stress levels are observed at location (2), Motor Mount Beam (30 MPa), location (1), Left Support Beam Bottom (35 MPa), and location (4), Right Support Beam Bottom (24 MPa).

Although Region 3 experiences the highest stress, the safety factor is still 3.2 against yielding. However, compared to Regions 1 and 2, this region is more utilised, and any reduction in material thickness should be approached with careful consideration, as this location is likely to limit the structural capacity of the support structure.

Note that all local maximum stresses presented above are below the yield strength of the material (see Table 2.1). The highest stress of 77 MPa occurs in Region 3, with a safety factor of 3.2 against yielding. The safety factors across all regions suggest that the current design is conservative.

3.1.1 Stress comparison between cases for 150-300 L

Since the geometry and load application points remain unchanged between load cases, the load paths remain mostly unchanged. Therefore, comparing the same

locations provides a valid basis for evaluating stress variations across cases. The evaluated points correspond to the locations defined in Figures 3.2-3.4. The results are presented in Figures 3.5-3.7.

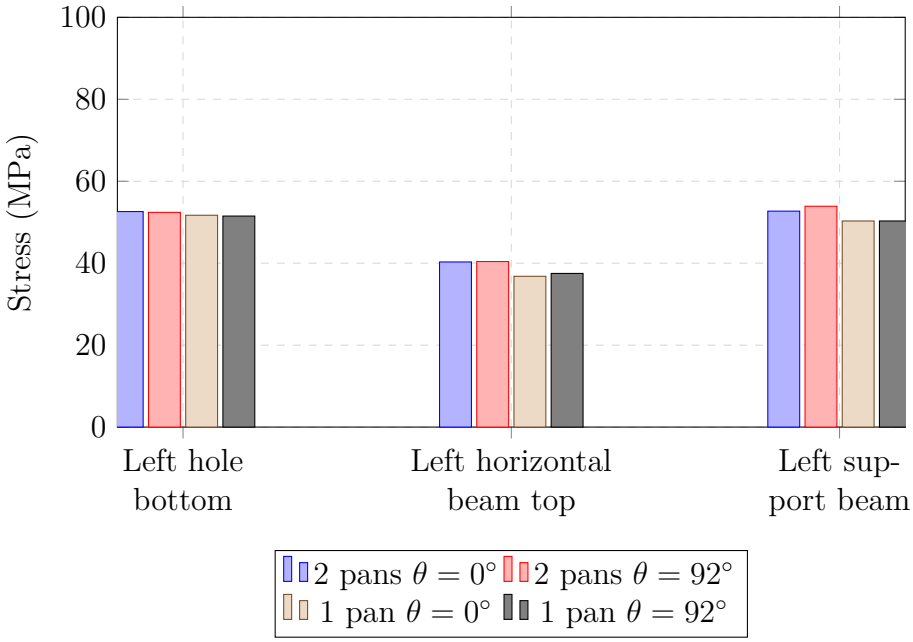

Figure 3.5: Comparison of von Mises stress values in Region 1 (see Figure 3.2) for the 150-300 L support structure.

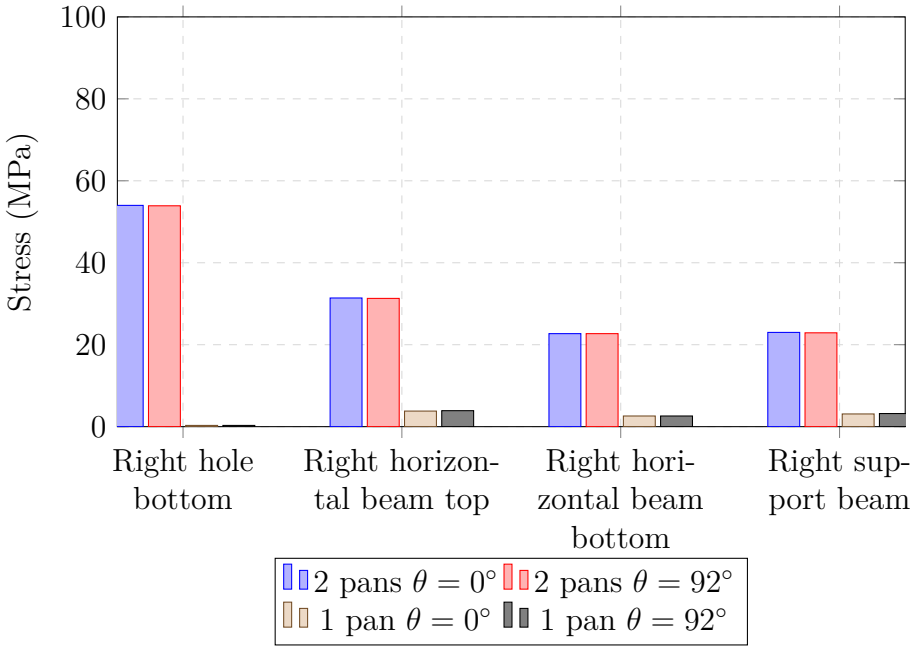

Figure 3.6: Comparison of von Mises stress values in Region 2 (see Figure 3.3) for the 150-300 L support structure.

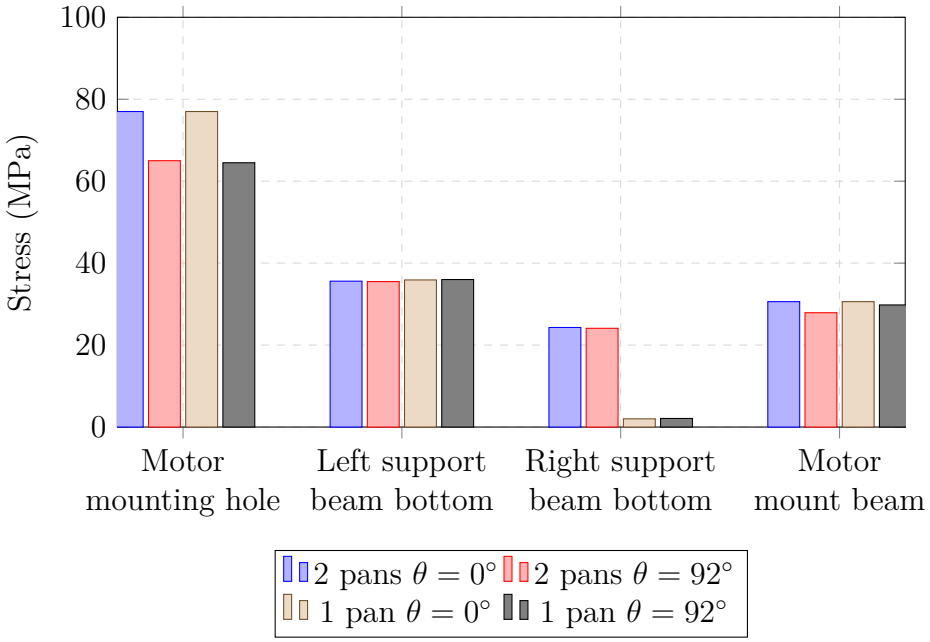

Figure 3.7: Comparison of von Mises stress values in Region 3 (see Figure 3.4) for the 150-300 L support structure.

Based on the Figures 3.5 - 3.7, the stress levels across the different load cases follow similar trends.

In Region 1, the stress levels vary only slightly across all load cases. This variation is due to minor differences in mesh discretization and the exact locations of the probe, as the applied loads in this region remain unchanged.

The single pan configurations show slightly lower stress levels. This can be attributed to the absence of loading on the right-side of the structure.

Region 2 follows a similar overall trend, but with a clear difference between single- and two-pan configurations. The stress levels show almost no variation between $\theta = 0°$ and $\theta = 92°$. This negligible influence of tilt angle suggests that load magnitude, rather than orientation, controls the structural response in this region.

In single-pan configurations, the stress levels are close to zero across all locations in Region 2, as no load is applied there. In two-pan configurations, the maximum stress reaches 54 MPa. Stress levels in region 2, therefore, depend if the structure is loaded in series.

Region 3 experiences the highest stress level (77 MPa) among all regions, with the motor mounting hole consistently being the most critical location. The maximum stress occurs for $\theta = 0°$, where the load magnitude in that area is highest. The remaining locations show consistent stress levels across load cases, except for the right support beam bottom, where the stress is close to zero for single-pan configurations due to no loading on the right side.

The results show that Region 3 consistently experiences the highest stress and is the critical region for this structure. Although the stress magnitudes may vary between load cases, the location of the critical area remains unchanged.

All stress levels are well below the material yield strength of 252 MPa, with a minimum safety factor of 3.2. The consistently high safety factors indicate potential over-dimensioning, suggesting that material reduction could be feasible without compromising structural integrity.

3.2 Stress Distribution for 50-100 L

Figure 3.8 shows the global stress distribution for the 50-100 L support structure under the most critical load case, i.e., two pans connected in series and mounted on the support structure with a tilt angle $\theta = 92°$.

The overall stress distribution follows the same pattern as for the 150-300 L support structure. The structure is divided into the same three regions as visible in Figure 3.8, with the previously defined evaluation locations used within each region.

Note that minor geometric differences are present in Region 3, where a single motor mount connection is used instead of two, and a small hole is present in the motor mount beam.

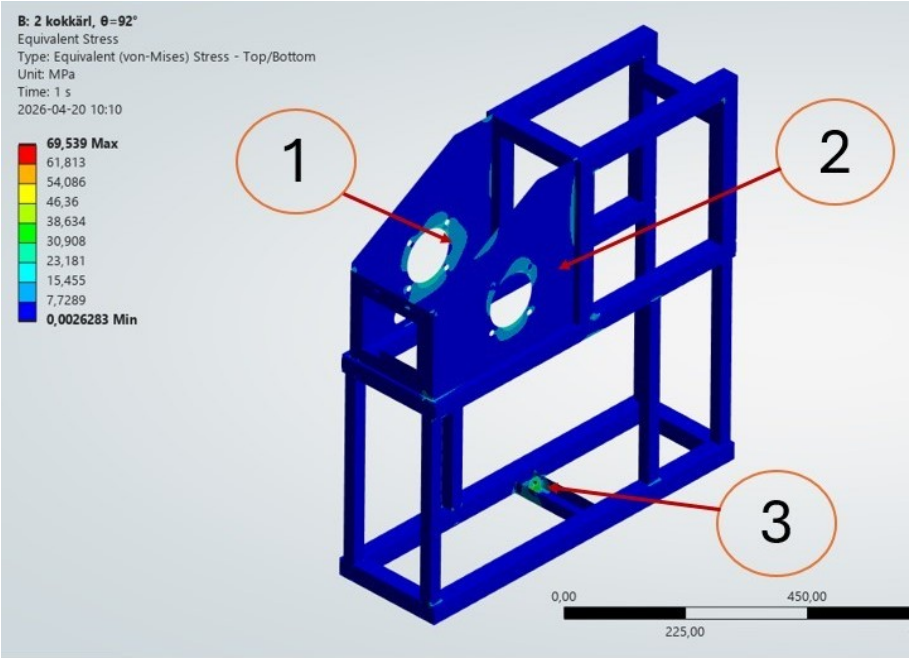

Figure 3.8: Isometric view of the 50-100 L support structure showing von Mises stress for the most critical load case. The highlighted general Regions (1-3) are examined in more detail in subsequent figures.

3.2.1 Stress comparison between load cases for 50-100 L

The same locations as previously defined in Figures 3.2-3.4, are used to compare stress variations across load cases. The results are presented in Figures 3.9-3.11.

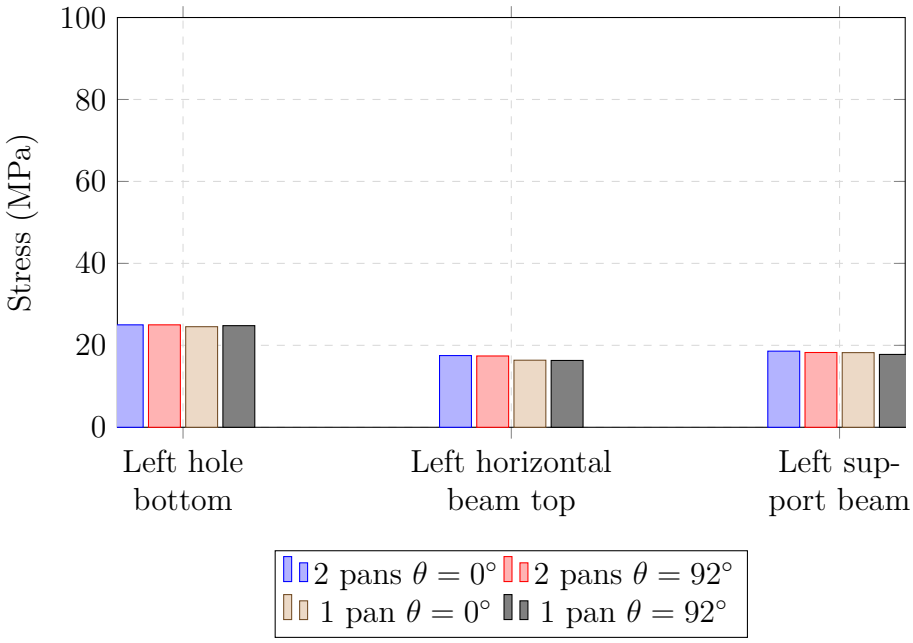

Figure 3.9: Comparison of von Mises stress values in Region 1 (see Figure 3.2) for the 50-100 L cases.

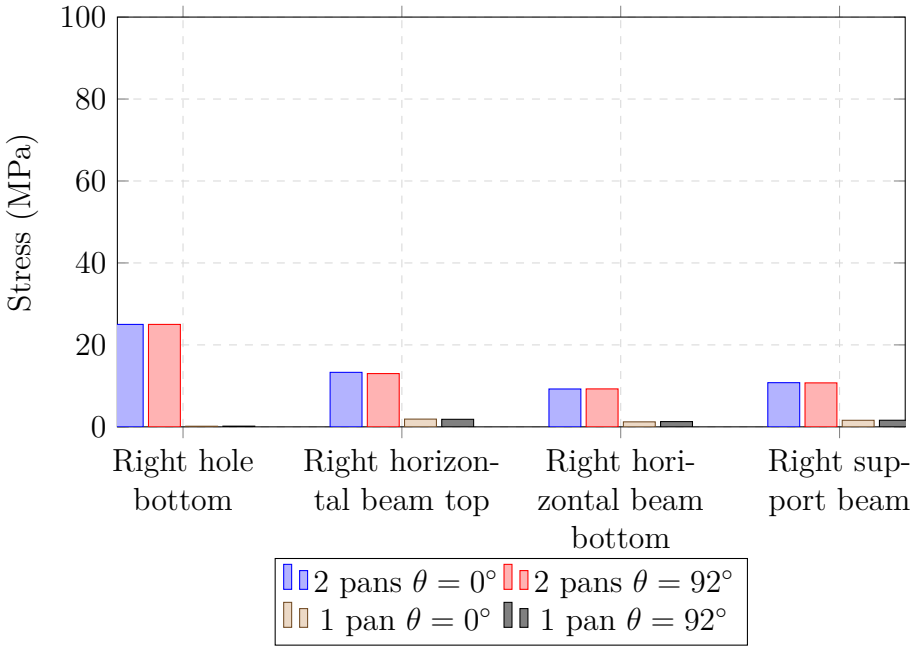

Figure 3.10: Comparison of von Mises stress values in Region 2 (see Figure 3.3) for the 50-100 L cases.

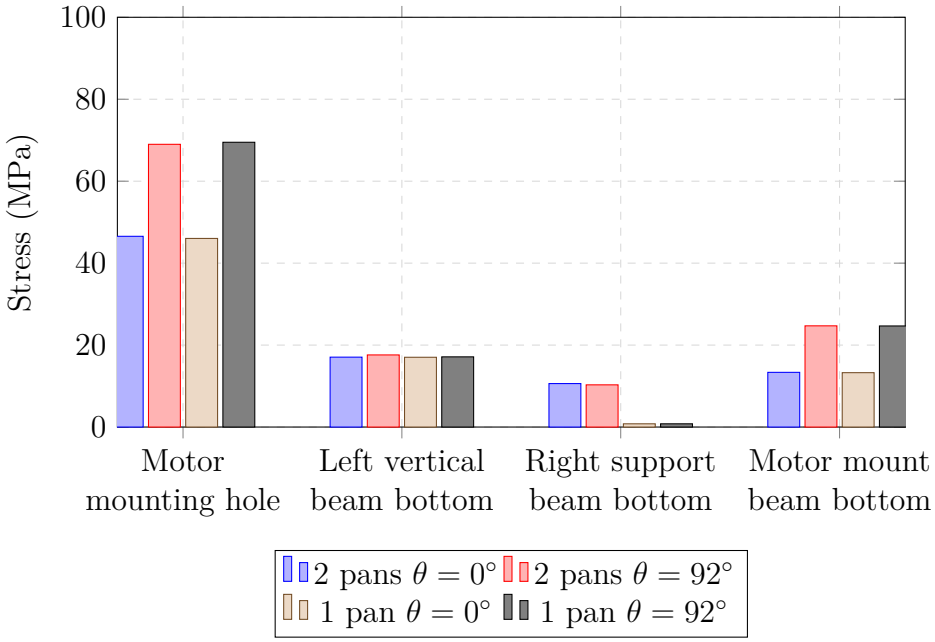

Figure 3.11: Comparison of von Mises stress values in Region 3 (see Figure 3.4) for the 50-100 L cases.

Based on Figures 3.9-3.11, the stress levels across the different load cases follow the same trends as those observed for the 150-300 L structure.

In Region 1, the stress levels are nearly identical across all load cases, with slightly lower stress levels in the single-pan configurations.

In Region 2, the stress is close to zero for single-pan configurations and increases in the two-pan cases. Similar to the 150-300 L structure, the stress is not influenced by the tilt angle.

In Region 3, the motor mounting hole remains the most critical location, with a maximum stress of 69 MPa. In contrast to the 150-300 L case, the highest stress occurs at $\theta = 92°$, which is consistent with loads increasing with θ at the motor mounting point for the 50-100 L structure.

Overall, the stress levels remain below the material yield strength, with a minimum safety factor of approximately 3.6 against yielding. This suggests potential for design optimisation, which is further investigated in the thickness sensitivity study.

3.3 Linear eigenvalue buckling analysis

A linear eigenvalue buckling analysis was performed to evaluate structural stability and identify potential buckling modes. The results showed similar buckling behaviour across all evaluated load cases, with local buckling occurring on the right and left side of the support structure.

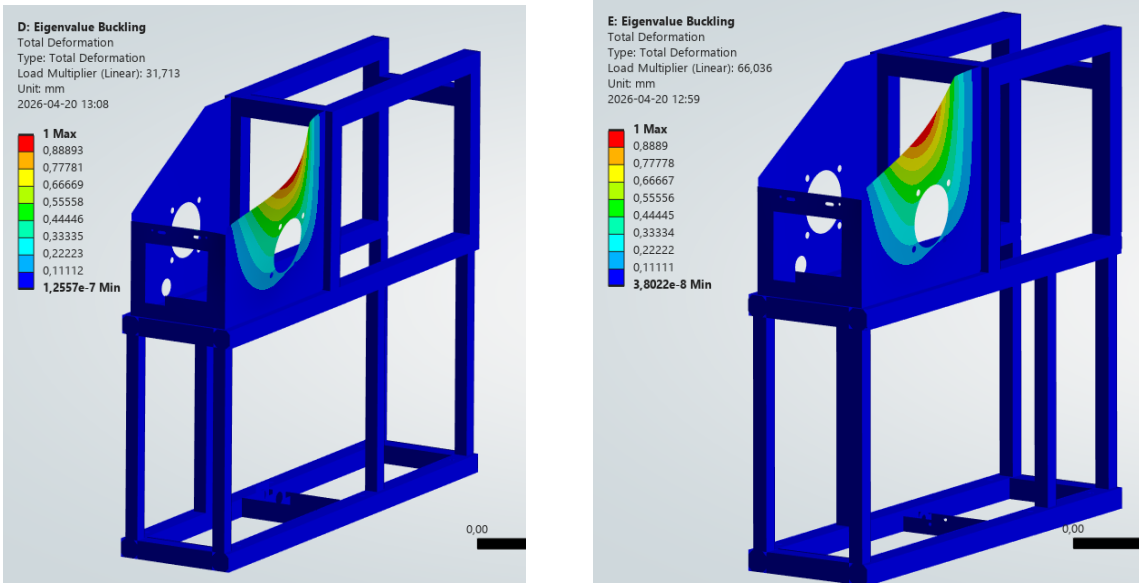

(a) 150–300 L **(b)** 50–100 L

Figure 3.12: Lowest buckling modes for the support structures: (a) 150-300 L and (b) 50-100 L. Both structures show similar buckling behaviour, with local buckling on the right side.

The lowest buckling modes for both support structures are shown in Figure 3.12.

For the 150-300 L support structure, the lowest load multiplier factor (LMF) is approximately 31 for the two-pan case and 45 for the single-pan case. For the 50-100 L support structure, the lowest LMF is approximately 66 for two-pan cases and 93 for the single-pan cases. The lower LMF in the 150-300 L support structure reflects a higher utilisation of the structure, as also seen in the stress levels.

In single-pan configurations, the lowest buckling mode shifts to the left side of the structure, with buckling to the right.

The relatively high load multiplier factors indicate that the structure is far from the critical buckling load under the applied loading conditions. However, it should be noted that these values are based on the assumptions of linear eigenvalue buckling analysis (see Section 2.6) and therefore represent theoretical buckling loads.

3.4 Maximum Total Deformation

The total deformation remains similar across all load cases, as the governing force on the left side of the structure remains unchanged. The maximum deformation, therefore, occurs at the same location in all cases.

For configurations with two pans, additional deformation is observed on the right side of the structure. Note that this deformation never exceeds the global maximum.

3.4.1 Maximum total deformation for 150-300 L

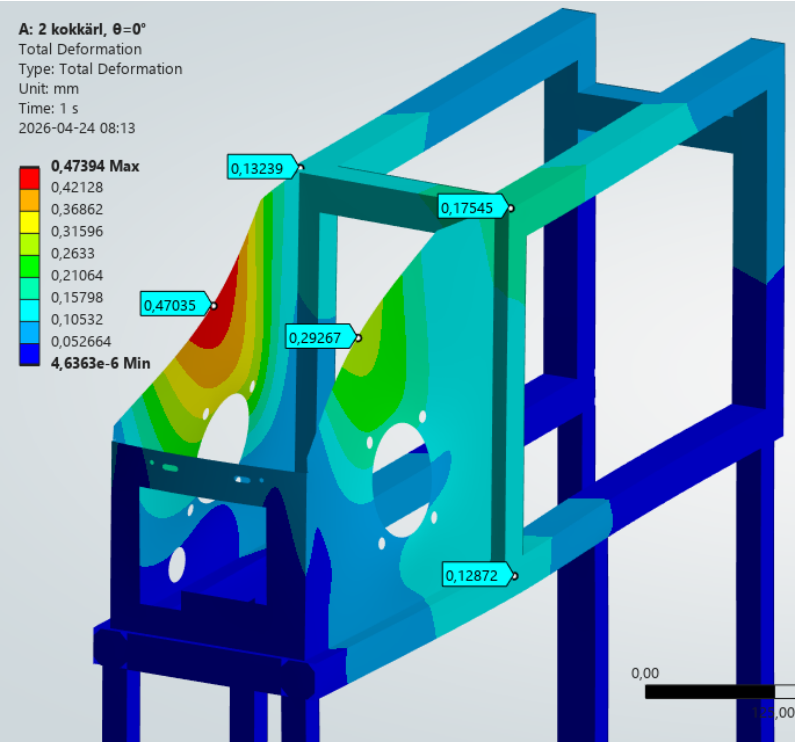

Figure 3.13: Maximum total deformation (0.47 mm) of the 150-300 L support structure for the most critical load case (2 pans $\theta = 0°$).

Figure 3.13 shows the total deformation for the load case resulting in the maximum total deformation. The maximum total deformation is approximately 0.47 mm and occurs for the two-pan configurations. The total deformation occurs at the same location and direction for all load cases. For the single-pan configurations, the maximum total deformation is approximately 0.35 mm.

The maximum deformation of 0.47 mm is small relative to the overall dimensions of the structure (848 mm x 247 mm) and is unlikely to affect functionality or alignment. In reality, additional structural elements such as sheet metal cladding and display braces are expected to further increase stiffness and reduce deformation.

3.4.2 Maximum total deformation for 50-100 L

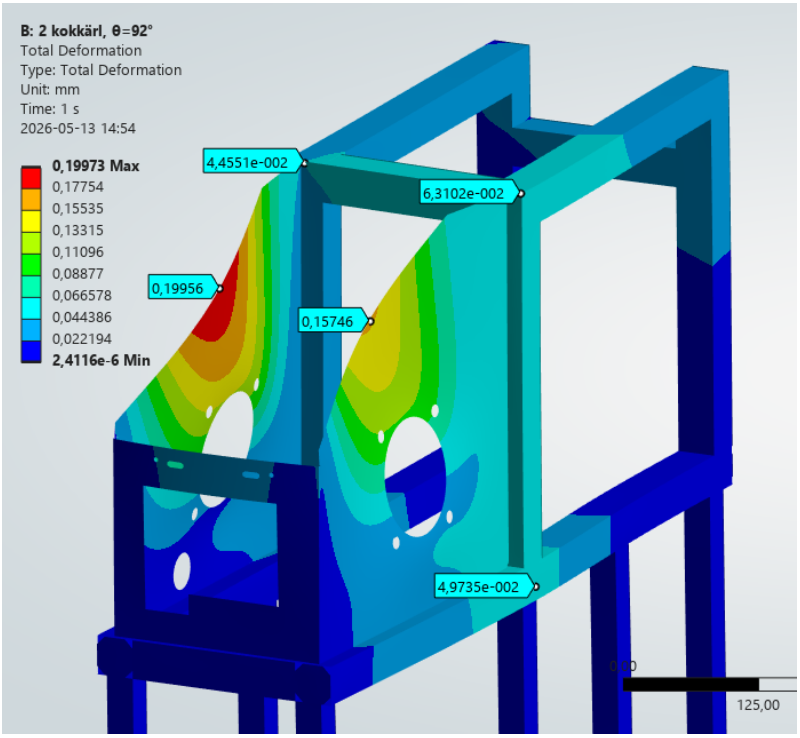

Figure 3.14: Maximum total deformation (0.2 mm) of the 50-100 L support structure for the most critical load case (2 pans $\theta = 92°$).

Figure 3.14 shows the total deformation for the load case resulting in the maximum total deformation. The maximum total deformation is approximately 0.20 mm and occurs for the two-pan configurations. The total deformation occurs at the same location and direction for all load cases. For the single-pan configurations, the maximum deformation is approximately 0.15 mm.
The maximum deformation of 0.20 mm is small relative to the overall dimensions of the structure and is unlikely to affect functionality or alignment. This is consistent with the behaviour observed for the 150-300 L structure.

3.5 Thickness Sensitivity Study

The previous analyses showed low stress levels and small deformations for both support structures. In addition, the buckling analysis yielded high LMF, further indicating potential for reduced material thickness. A thickness sensitivity study was therefore performed.

In this study, the same loads, boundary conditions, mesh settings, and evaluation locations as in the original analyses were used. The thickness of the RHS was varied from 3 mm (original) down to 1.5 mm because it appears to be less utilised compared to the sheet metal. The sheet metal thickness was kept constant to isolate the effect of reduced RHS thickness.

The reduction of mass was calculated for each thickness and size.

Table 3.1: Estimated mass reduction of the support structures for different RHS thicknesses.

Structure size	**RHS thickness [mm]**	**Total mass [kg]**	**Mass reduction [%]**
150-300 L	3.0	40.12	0
	2.0	29.62	26.17
	1.5	24.37	39.25
50-100 L	3.0	36.20	0
	2.0	26.76	26.07
	1.5	22.04	39.11

According to Table 3.1, significant mass reductions can be achieved by reducing the thickness of the RHS beams.

3.5.1 Thickness sensitivity results for 150-300 L

The thickness sensitivity study was performed for the reduced RHS thicknesses of 2 mm and 1.5 mm, corresponding to standard available dimensions.

For each thickness, the maximum stress, the maximum total deformation, and the minimum LMF were determined for all load cases. The results are summarised in Table 3.2.

Table 3.2: Comparison of structural response for different thicknesses and load cases for the 150-300 L support structure.

Load case	**RHS Thickness [mm]**	**Max stress [MPa]**	**Max deformation [mm]**	**Min LMF [-]**
2 pans, $\theta = 0°$	3.0	77	0.47	31
	2.0	90	0.55	27
	1.5	127	0.65	24
2 pans, $\theta = 92°$	3.0	65	0.47	31
	2.0	93	0.55	27
	1.5	127	0.64	24
1 pan, $\theta = 0°$	3.0	77	0.35	45
	2.0	85	0.36	34
	1.5	115	0.37	27
1 pan, $\theta = 92°$	3.0	64	0.35	45
	2.0	84	0.36	34
	1.5	120	0.37	27

The results in Table 3.2 show that reducing the RHS thickness from 3 mm to 2 mm has a relatively small effect on the structural response. The increase in stress, deformation, and reduction in LMF is relatively small, and the overall behaviour remains similar across all load cases. This suggests that the structure is not highly sensitive to thickness reduction within this range.

However, this is not the case when the thickness is further reduced to 1.5 mm. The maximum stress increases from 90 MPa to 127 MPa, resulting in a safety factor of approximately two. This significant increase in stress shows that the structure becomes more sensitive to thickness reduction below 2 mm.

The increase in stress is largest in previously defined regions where smaller RHS beams connect to larger ones. In these locations, the load is partly transferred through the face of the larger beam, causing local plate bending. As the thickness is reduced, the bending stiffness decreases, leading to rapid increases in stress in these areas. The most stressed location in every load case with a thickness of 2 mm or below is location 3 in Region 1, visible in Figure 3.2.

The deformation follows the same trend and location as Section 3.4. The maximum deformation occurs at the same location for all thicknesses and load cases. The structures flexibility increases as the thickness is reduced, and additional deformation can be seen in the left and right support beams. However, the reduction in thickness primarily affects the magnitude of deformation rather than its location.

The LMF decreases with reduced thickness but remains relatively high for all cases. This suggests that buckling is not the limiting factor, even for reduced thicknesses.

The results show that stress is the limiting factor when optimising the structure.

3.5.2 Thickness sensitivity results for 50-100 L

The thickness sensitivity study for the 50-100 L support structure was carried out using the same approach as for the 150-300 L structure. The results are summarised in Table 3.3.

Table 3.3: Comparison of structural response for different thicknesses and load cases for the 50-100 L support structure.

Load case	**RHS Thickness [mm]**	**Max stress [MPa]**	**Max deformation [mm]**	**Min LMF [-]**
2 pans, $\theta = 0°$	3.0	46	0.2	66
	2.0	46	0.22	57
	1.5	51	0.25	50
2 pans, $\theta = 92°$	3.0	69	0.2	66
	2.0	69	0.22	57
	1.5	69	0.25	50
1 pan, $\theta = 0°$	3.0	46	0.15	93
	2.0	46	0.15	72
	1.5	51	0.16	59
1 pan, $\theta = 92°$	3.0	69	0.15	93
	2.0	69	0.15	72
	1.5	69	0.16	59

The results in Table 3.3 show that reducing the RHS thickness has a small effect on the structural response for the 50-100 L support structure.

For all load cases, the maximum stress remained practically unchanged when the thickness is reduced from 3 mm to 1.5 mm, but local stress increases are observed throughout the structure. For the $\theta = 92°$ cases, the maximum stress remains constant at 69 MPa for all thicknesses because the stress in other regions only increased to a maximum of 51 MPa. For the $\theta = 0°$ cases, the stress increased from 46 to 51 MPa, with the most loaded area being location 3 in Region 1, consistent with the local plate bending behaviour observed for the 150-300 L structure.

The deformation increased slightly with reduced thickness, from 0.20 mm to 0.25 mm for the two-pan configurations and from 0.15 mm to 0.16 mm for the single-pan

configurations. Similar to the 150-300 L structure, the reduction in thickness primarily affects the magnitude of deformation rather than its location.

The LMF decreases with reduced thickness but remains relatively high for all cases. Just as the 150-300 L structure, this suggests that buckling is not the limiting factor, even for reduced thicknesses.

The results show that the 50-100 L structure is less sensitive to thickness reduction compared to the 150-300 L structure.

4
Concluding remarks

4.1 Summary of Key Findings

The structural analyses show that both support structures are conservatively dimensioned under the considered load cases, thus directly addressing the research question regarding structural utilisation. All stress levels remain below the material yield strength of 252 MPa, with minimum safety factors of approximately 3.2 for the 150-300 L structure and 3.6 for the 50-100 L structure.

The motor mounting hole in Region 3 is identified as the most critical location for both structures. This is consistent across all load cases.

Deformations are considered small, and buckling has high LMFs.

The thickness sensitivity study shows that the 150-300 L structure is sensitive to thickness reductions of RHS beams below 2 mm, with stress levels increasing significantly. In comparison, the 50-100 L structure is less sensitive and shows no significant increase in stress levels when the RHS beam thickness is reduced from 3 mm to 1.5 mm.

4.2 Discussion of Results

The 150-300 L structure is already well balanced in its current design. Although the stress levels are relatively low, the safety factor of 3.2 provides a reasonable margin considering the uncertainties in the analyses, such as neglected dynamic effects and simplified loading conditions.

Any reduction in the RHS thickness would improve material efficiency but also reduce the safety factor. Since the analysis does not include dynamic loading, further reduction of this margin may be hard to justify.

For the 50-100 L structure, the behaviour is different. Reducing the thickness has a small effect on the maximum stress across load cases. This suggests that some material reduction may be possible. However, since dynamic effects are not evaluated, this should be considered with caution.

The results show that thickness reduction may not be the most effective optimisation strategy. Reducing the RHS thickness will reduce material usage by 26-29%, but it comes with reduced safety factors, which are undesirable. A more relevant economic improvement may therefore be to redesign the support structure with a focus on manufacturing efficiency, fewer welded joints, and simpler assembly.

The study has also clearly identified the most critical regions of the structures. This information is valuable for Steeltech from both manufacturing and maintenance perspectives since it shows where weld quality is most important and which areas should receive extra attention during inspections and service.

4.3 Limitations

The model is based on the modelling assumptions described in Section 2.3.2. The following discusses how these assumptions influence the results.

The loads are applied as static forces at the mounting points. In reality, the system includes both a tilting motor and an internal mixing motor, which introduces loads that vary with time. The internal mixing also generates additional torque that must be balanced by the support structure. These dynamic effects may also introduce horizontal loading that pushes the supporting structure laterally. None of these contributions are included in the current model and may lead to an underestimation of the structural loading.

This horizontal loading can also reduce the structures resistance to buckling. The buckling analysis, as previously mentioned in Section 2.6, is based on idealised models with perfect geometry. Geometric imperfections, such as geometric deviations, are always present, further reducing the buckling capacity. As a result, the actual LMF may be lower than those predicted by the analysis.

However, since the lowest predicted LMF is relatively high (approximately 31 and 66), the structure is still subjected to loads far below the critical buckling load under the considered conditions.

The weight of auxiliary components such as cables, electrical boxes, and the tilting motor is also not modelled explicitly. These contributions are estimated to be less than 12% of the total load and were therefore well accounted for by the load factor of 1.35. This simplifies the model but may slightly underestimate the total applied load on the structure. The applied loads were scaled according to Eurocode 0 (SS-EN 1990:2023) (Svenska institutet för standarder (SIS), 2023) to provide a more conservative analysis.

Despite the simplifications listed above, the model captures the main load paths and is sufficient for comparing load cases, evaluating thickness changes, analysing stresses, deformations, and structural stability. However, the exact values should be interpreted with some caution.

4.3.1 Boundary Conditions

The use of frictionless support implies that no horizontal forces are transferred through the contact surface via friction. This results in all in-plane loads being carried by the bolt hole constraints, which may lead to a slight overestimation of stresses in these regions.

Additionally, since twisting of the support may occur and the frictionless support would hinder this, force probes were extracted from the underside of the structure. No twisting behaviour was observed (see Appendix B Figures B.2 and B.3 for examples), indicating that this modelling simplification has a limited impact on the results.

The load application at the motor mounting holes is represented using distributed forces. A bearing-load representation would more accurately capture the local contact behaviour, but this is not compatible with the mid-surface modelling approach used in this study.

Since the maximum stress occurs at the inside of the motor mounting hole, this modelling approach may influence the reported maximum stress values. The distributed force applies load over the selected surface rather than as a contact pressure. The local stress values at the motor mounting hole should therefore be interpreted with some caution. However, the results consistently identify the motor mounting region as the critical area, even if the exact local stress value may be influenced by the boundary condition. Since this region is identified as critical, careful execution of the welds here is of importance.

Overall, the boundary conditions are considered to provide a realistic representation of the structural behaviour while maintaining a reasonable modelling complexity.

4.4 Recommendations and Future Work

The results show that both structures are adequately designed, providing sufficient safety factors without being excessively conservative. No immediate changes are required to ensure safe operation under the considered load cases.

For the 150-300 L structure, further material reduction is not recommended due to reduced safety factors and modelling uncertainties.

For the 50-100 L structure, material reduction may be possible but should be evaluated with consideration of dynamic effects.

Future work should focus on manufacturing and design aspects, such as reducing welding steps, improving production efficiency, and evaluating alternative structural layouts to minimise cost.

4.5 Final conclusions

The results are reliable for evaluating structural performance and supporting engineering decisions regarding the structure. The support structures are safe under the considered load cases and fulfil the requirements for structural performance. The 150-300 L support structure is appropriately dimensioned, while the 50-100 L structure shows some potential for further optimisation. Overall, the current designs provide a good balance between safety and material usage.

References

Ansys, Inc. (2024a). *Ansys SpaceClaim* (Version Release 2) [Computer software]. https://www.ansys.com/products/3d-design/ansys-spaceclaim

Ansys, Inc. (2024b). *Ansys spaceclaim help: Shared topology*. Retrieved March 1, 2026, from https://ansyshelp.ansys.com/account/secured?returnurl=/Views/Secured/corp/v242/en/spaceclaim/Discovery/user_manual/st_sharetopology.html#c_sharing_topology

Ansys, Inc. (2024c). *Ansys Workbench* (Version Release 2) [Computer software]. https://www.ansys.com/products/ansys-workbench

Ansys, Inc. (2026). *Ansys granta edupack* [Accessed: 2026-03-16]. Ansys. https://www.ansys.com/products/materials/granta-edupack

Autodesk, Inc. (2026). *Autodesk inventor* [Computer software]. https://www.autodesk.com/products/inventor

COMSOL AB. (2014). *Buckling: When structures suddenly collapse*. Retrieved April 22, 2026, from https://www.comsol.com/blogs/buckling-structures-suddenly-collapse

Davis, J., Clark, M., Cofer, D., Fifarek, A., Hinchman, J., Hoffman, J., Hulbert, B., Miller, S., Wagner, L., & Collins, R. (2013). Study on the barriers to the industrial adoption of formal methods. *Lecture Notes in Computer Science*, *8187*, 63–77. https://doi.org/10.1007/978-3-642-41010-9_5

Eckert, C., & Ola, I. (2017). Safety margins and design margins: A differentiation between interconnected concepts. *Procedia CIRP*, *60*, 267–272. https://doi.org/10.1016/j.procir.2017.03.140

Jagota, V., Sethi, A. P. S., & Kumar, K. (2013). Finite element method: An overview. *Walailak Journal of Science and Technology*, *10*(1), 1–8. https://wjst.wu.ac.th/index.php/wjst/article/view/499

O'Driscoll, M. (2002). Design for manufacture. *Journal of Materials Processing Technology*, *122*. https://www.sciencedirect.com/science/article/abs/pii/S0924013601011323

Rexander, A. (2026, January). Personal communication with steeltech i alingsås ab.

Saravacos, G., & Kostaropoulos, A. E. (2016). *Handbook of food processing equipment*. Springer International Publishing. https://doi.org/10.1007/978-3-319-25020-5

Steeltech i Alingsås AB. (2026a). *Mixomat* [Accessed: 2026-02-02]. https://www.steeltech.se/industri/industrigrytor/mixomat/

Steeltech i Alingsås AB. (2026b). *Om steeltech* [Accessed: 2026-02-02]. https://www.steeltech.se/om-steeltech/

Svenska institutet för standarder (SIS). (2023). SS-EN 1990:2023 eurocode – basis of structural design [Accessed: 2026-03-17; establishes principles for structural design and partial safety factors]. https://www.sis.se/en/produkter/construction-materials-and-building/construction-industry/technical-aspects/ssen19902

Swedish Institute for Standards. (2005). *Ss-en 13886:2005+a1:2010 food processing machinery: Cooking kettles equipped with powered stirrer and/or mixer: Safety and hygiene requirements* (tech. rep.). SIS Förlag. Stockholm. Retrieved January 27, 2026, from https://www.sis.se/en/produkter/maskinsakerhet-357f77b1/food-processing-machinery-/ssen138862005a12010

U.S. Environmental Protection Agency. (2023). *Watersense at work – commercial steam kettles*. Retrieved January 27, 2026, from https://www.epa.gov/system/files/documents/2023-05/ws-commercial-watersense-at-work_Section_4.5_Steam_Kettles.pdf

Zienkiewicz, O. C., & Taylor, R. L. (2005). *The finite element method: Its basis and fundamentals* (6th ed.). Elsevier Butterworth-Heinemann.

A

Python Script for Load Calculations

The following script was used to calculate the loads for each tilt angle θ.

```
"Parts of the code were developed with assistance from AI-based tools.
The generated code was reviewed, modified, and validated
by the author before use in the analysis."
import numpy as np
import matplotlib.pyplot as plt
from matplotlib.widgets import Slider

# PARAMETRAR

A_x, A_y = 0.0, 0.0        # Kopplingspunkt motor (origo)
P_x, P_y = -0.2283, 0.5761 # Rotationspunkt för hävarm relativ origo
L_small = 0.145            # Hävarmens längd
alpha0 = np.radians(-26.9) # Hävarmens lutning i starten
m = 557*1.5                # massa med lastfaktor
g = 9.81                   # gravitation (m/s^2)
F_g = m * g                # kraft (N)
L_r = 0.4933               # Hävarm till masscentrum för kokkärlet i meter
alpha_r_deg = -33.8        # startvinkel hävarm för masscentrum i deg
theta_min, theta_max = 0, 92 # Lutningsintervall för kokkärlet

# FUNKTIONER

def C_theta(theta_deg):
    "Beräknar kopplingspunkt C för given lutningsvinkel."
    theta_rad = np.radians(theta_deg)
    C_x = P_x + L_small * np.cos(alpha0 + theta_rad)
    C_y = P_y + L_small * np.sin(alpha0 + theta_rad)
    return C_x, C_y

def CM_theta(theta_deg):
    "Beräknar masscentrumets position."
    alpha_rad = np.radians(alpha_r_deg + theta_deg)
    CM_x = P_x + L_r * np.cos(alpha_rad)
    CM_y = P_y + L_r * np.sin(alpha_rad)
```

```
    return CM_x, CM_y

def moment(theta_deg):
    "Beräknar momentet från tyngdkraften kring rotationspunkten P."
    alpha_rad = np.radians(alpha_r_deg + theta_deg)
    return F_g * L_r * np.cos(alpha_rad)

def angles(theta_deg):
    "Beräknar vinklar"
    C_x, C_y = C_theta(theta_deg)
    phi = np.arctan2(C_y, C_x)
    psi = np.arctan2(C_y - P_y, C_x - P_x)
    gamma = np.abs(phi - psi)
    if gamma > np.pi:
        gamma = 2 * np.pi - gamma
    phi_deg = np.degrees(phi)
    psi_deg = np.degrees(psi)
    gamma_deg = np.degrees(gamma)
    return phi, psi, gamma, phi_deg, psi_deg, gamma_deg

def force(theta_deg):
    "Kraft från momentjämvikt:"
    "F = M/momentarm, vilket är ekvivalent med"
    "M = r x F där momentarmen motsvarar |PC x (AC/|AC|)|"
    _, _, gamma, _, _, _ = angles(theta_deg)
    a = L_small
    M = moment(theta_deg)
    F = M / (a * np.sin(gamma))
    return F

# FIGUR

theta0 = 0
fig, (ax1, ax2) = plt.subplots(1, 2, figsize=(12, 5))
plt.subplots_adjust(bottom=0.25)

ax1.set_aspect('equal')
ax1.set_xlim(-0.7, 0.7)
ax1.set_ylim(-0.2, 1.2)
ax1.grid(True)
ax1.set_title("Geometry")

C0_x, C0_y = C_theta(theta0)
CM0_x, CM0_y = CM_theta(theta0)

line1, = ax1.plot([A_x, C0_x], [A_y, C0_y], 'b', lw=2)
```

```
line2, = ax1.plot([P_x, C0_x], [P_y, C0_y], 'r', lw=2)
pointA, = ax1.plot(A_x, A_y, 'ko')
pointP, = ax1.plot(P_x, P_y, 'ko')
pointC, = ax1.plot([C0_x], [C0_y], 'go', markersize=6)

line_CM, = ax1.plot([P_x, CM0_x], [P_y, CM0_y], 'g--', lw=2)
pointCM, = ax1.plot([CM0_x], [CM0_y], 'mo', markersize=6)
text_CM = ax1.text(CM0_x + 0.01, CM0_y + 0.01, "Masscentrum",
color='Black')

text_A = ax1.text(A_x + 0.01, A_y + 0.01, "A", fontsize=10,
fontweight='bold', color='black')
text_P = ax1.text(P_x - 0.03, P_y + 0.01, "P", fontsize=10,
fontweight='bold', color='black')
text_C = ax1.text(C0_x + 0.01, C0_y + 0.01, "C", fontsize=10,
fontweight='bold', color='green')

text_force = ax1.text(0.02, 0.98, "", transform=ax1.transAxes,
va='top', ha='left',
bbox=dict(facecolor='white', alpha=0.85,
edgecolor='none'))
text_angle = ax1.text(0.98, 0.98, "",transform=ax1.transAxes,
va='top',ha='right',fontsize=10,
fontweight='bold',
bbox=dict(facecolor='white', alpha=0.9,
edgecolor='white'))
text_components = ax1.text(0.02, 0.02, "",
transform=ax1.transAxes, va='bottom', ha='left',
bbox=dict(facecolor='white', alpha=0.85, edgecolor='none'))

plt.grid(True)
ax2.set_title("Force vs Tilt angle")
theta_vals = np.linspace(theta_min, theta_max, 300)
F_vals = np.array([force(t) for t in theta_vals])
lineF, = ax2.plot(theta_vals, F_vals, 'b', label='Kraft (N)')
ax2.set_xlabel("Theta (Degrees)")
ax2.set_ylabel("Force (N)")
ax2.spines['right'].set_visible(False)

# SLIDER

ax_slider = plt.axes([0.25, 0.1, 0.5, 0.03])
slider = Slider(ax_slider, 'Theta (Degrees)', theta_min,
theta_max, valinit=theta0)

def update(val):
```

```
    theta = slider.val
    C_x, C_y = C_theta(theta)
    CM_x, CM_y = CM_theta(theta)

    line1.set_data([A_x, C_x], [A_y, C_y])
    line2.set_data([P_x, C_x], [P_y, C_y])
    line_CM.set_data([P_x, CM_x], [P_y, CM_y])

    pointC.set_data([C_x], [C_y])
    pointCM.set_data([CM_x], [CM_y])
    text_C.set_position((C_x + 0.01, C_y + 0.01))
    text_CM.set_position((CM_x + 0.01, CM_y + 0.01))

    F_now = force(theta)
    phi_rad, psi_rad, gamma_rad, phi_deg, psi_deg, gamma_deg = angles(theta)
    angle_to_show = 180 - phi_deg
    angle_use = np.pi - phi_rad
    Fx = F_now * np.cos(angle_use)
    Fy = F_now * np.sin(angle_use)

    text_force.set_text(f"Total Force: {F_now:,.1f} N")
    text_components.set_text(f"Fx = {Fx:,.1f} N\nFy = {Fy:,.1f} N")
    text_angle.set_text(f"fi {angle_to_show:.2f}°")
    fig.canvas.draw_idle()
slider.on_changed(update)
update(theta0)
plt.show()
```

B

Additional Figures

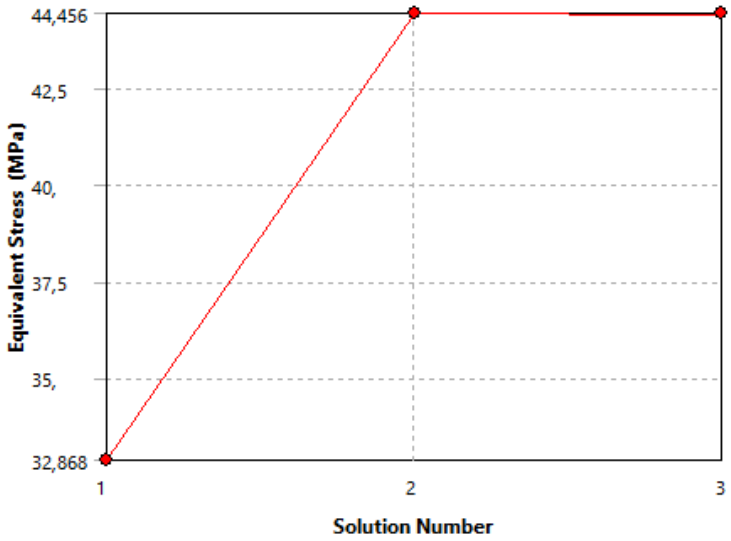

Figure B.1: Example of mesh convergence study showing the variation of von Mises stress with decreasing element size. The stress curve flattens as the mesh is refined, meaning that the solution has converged.

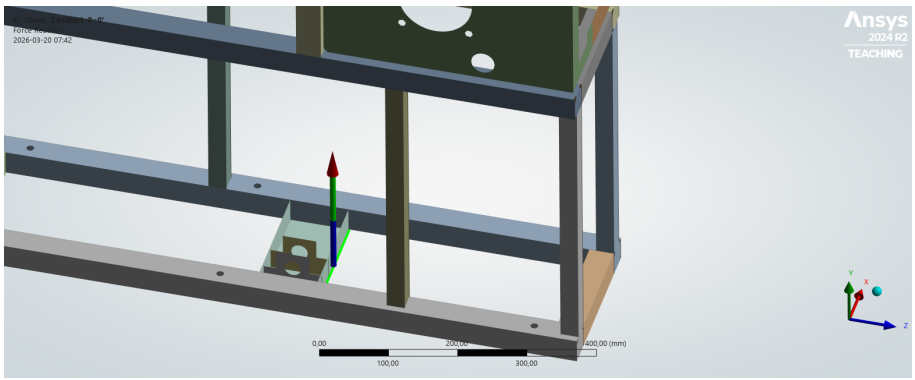

Figure B.2: Force reaction of tilting motors mounting plate, front side.

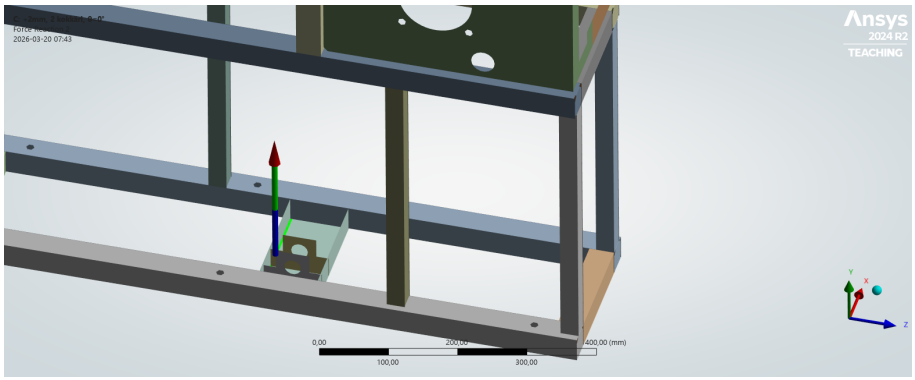

Figure B.3: Force reaction of tilting motors mounting plate, back side.

C

Load case forces

To understand the following force directions, the Cartesian coordinate directions will be explained. The front of the cooking pan in Figure 2.2 is pointing towards the positive $z-$direction. Pointing up, you get the positive $y-$direction. The positive $x-$direction is pointing towards the right in the figure.

Table C.1: Applied forces for the representative load cases. Remote Force and Force components (X, Y, Z) are listed for each case. All forces are scaled according to Eurocode 0 (SS-EN 1990:2023) (Svenska institutet för standarder (SIS), 2023). If a square is left empty there is no force in that direction.

Acceleration is 13.2435 m/s^2 for every load case				
100L support structure				
Load Case	**Force Type**	**X [N]**	**Y [N]**	**Z [N]**
Single pan, $\theta = 0°$	Remote Force Left		-1890,87	
	Force		-6751,8	-1224,5
Single pan, $\theta = 92°$	Remote Force Left		-1890,87	
	Force		-9811,2	-2209,8
Two pans in series, $\theta = 0°$	Remote Force Left		-1890,87	
	Remote Force Right		-1890,87	
	Force		-6751,8	-1224,5
Two pans in series, $\theta = 92°$	Remote Force Left		-1890,87	
	Remote Force Right		-1890,87	
	Force		-9811,2	-2209,8
300L support structure				
Load Case	**Force Type**	**X [N]**	**Y [N]**	**Z [N]**
Single pan, $\theta = 0°$	Remote Force Left		-4098,12	
	Force		-28819,7	-5588
Single pan, $\theta = 92°$	Remote Force Left		-4098,12	
	Force		-23124,5	-5465,6
Two pans in series, $\theta = 0°$	Remote Force Left		-4098,12	
	Remote Force Right		-4098,12	
	Force		-28819,7	-5588
Two pans in series, $\theta = 92°$	Remote Force Left		-4098,12	
	Remote Force Right		-4098,12	
	Force		-23124,5	-5465,6

Department of Industrial and Materials Science
CHALMERS UNIVERSITY OF TECHNOLOGY
Gothenburg, Sweden
www.chalmers.se

CHALMERS